Submission code: KRP0P69GR0

See this and other abstracts on our website: https://home.sbgf.org.br/Pages/resumos.php

Anisotropy and accuracy analysis in the processing of 3D4C SS-wave seismic data

Yuanyuan Yue (BGP; CNPC), Pengyuan Sun (BGP; CNPC), Xiangyang Li (BGP; CNPC), Hongmei Nie (BGP; CNPC), Jianlei Zhang (BGP; CNPC), Qianggong Song (BGP; CNPC)

Anisotropy and accuracy analysis in the processing of 3D4C SS-wave seismic data

Abstract

This paper summarizes practical criteria for anistropy and accuracy analysis method in the processing of 3d4C SS-wave seismic data. These approaches were illustrated using synthetic data and subsequently applied to field data from a 3D9C survey. The results show that the subsurface is azimuthally anisotropic, and the polarization directions of S1 don't vary with depth, and the computed fracture orientations are sufficiently accurate, therefore, the S1S1/S2S2 separation results are reliable.

Introduction

4C SS-wave seismic exploration can be dated back to the 1980s. Since the subsurface often exhibits azimuthal anisotropy induced by alighned fractures or cracks, the processing of 4C SS-wave data ofen faces the problem of calculating the fracture orientation (S1 polarization direction) and separating fast/slow shear waves. To do this, Alford proposed a rotation method in 1986, and Li and Crampin proposed a linear transformation method in 1991. Recently, BGP conducted 3D9C seismic exploration and the 4C SS-wave data was processed and good imaging results of S1S1 and S2S2 were obtained. This paper provide a summary of the criteria for anisotropy and accuracy analysis method in the processing of 4C SS-wave data form the 3D9C survey.

Method

Two horizontal excitations(generally in X and Y directions) and one vertical excitation are adopted in 3D seismic exploration, and for each excitation, recorded by two horizontal geophones(again in X and Y directions) and one vertical geophone, giving rise to 3D9C seismic data. Select the 4C data (SxRx, SxRy, SyRx and SyRy) excited and recorded in X-Y directions, and process them to get the SS-wave imaging results. During the 4C SS-wave data processing, many analysis work is required and the three key steps are as follows:

1. To determine whether the subsurface is azimuthally isotropic or not

Although subsurface media are usually azimuthally anisotropic, the existence of azimuthally isotropic cases cannot be ruled out, such as the Lungu survey in China. So we should first rotate the observation directions of 4C SS-wave data to R-T directions from X-Y directions using formula (1): $\mathbf{Q} = \mathbf{R}^{\mathbf{T}}(\boldsymbol{\partial})\mathbf{P}\mathbf{R}(\boldsymbol{\partial})$ (1)

Define the inline direction as 0 degrees, and denote the direction of R (source to receiver) as ∂, which can be calculated according to the coordinates of the source point and the receiver point. Where $R(\partial) = \begin{bmatrix} cos\partial & sin\partial \\ -sin\partial & \cos\partial \end{bmatrix}$, $P = \begin{bmatrix} SxRx & SxRy \\ SyRx & \mathrm{SyRy} \end{bmatrix}$, $Q = \begin{bmatrix} SrRr & SrRt \\ StRr & \mathrm{StRt} \end{bmatrix}$。 If the subsurface is azimuthally isotropic, the SV waves are distributed in the SrRr component, and the SH waves are distributed in the StRt component. There are no reflected waves in the SrRt and StRr components at any azimuth, as shown in Figure 1b, and the processing for shear wave splitting is not required. Otherwise, the reflected waves will occoured on SrRt and StRr components in most azimuths no matter how near the offset is, and the reflection events vary with azimuth, specifically showing shear wave splitting characteristics of polarity reversal with 90-degree intervals (see the orange box in Figure 1d). If the events of SrRt from different azimuths (as shown in Figure 4a) are stacked, the stacked section will be very weak due to the above-mentioned polarity reversal, as shown in

Figure 4b. And the same applies to the StRr component. Therefore, it is not reliable to judge the subsurface is azimuthally isotropic or anisotropic using 4C total stack sections. Instead, pre-stack 4C data or azimuth-stacked 4C data (as shown in Figure 4a) should be used for this judgment.

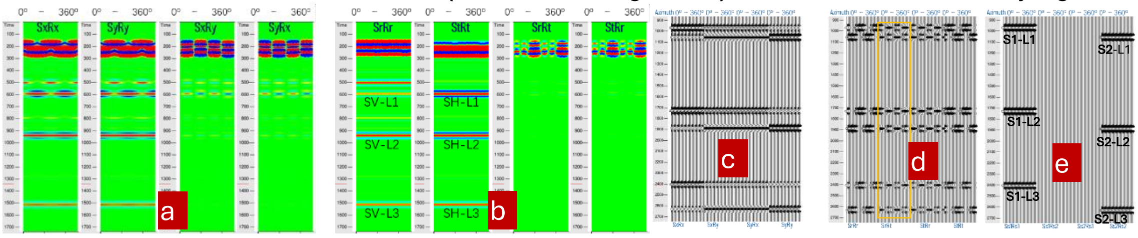

Figure 1: Common 50m offset 4C sythetic data of ISO model and HTI model. a: SxRx, SyRy, SxRy and SyRx components of ISO model. b: SrRr, StRt, SrRt and StRr components of ISO model. c: SxRx, SxRy, SyRx and SyRy components of HTI model. d: SrRr, SrRt, StRr and StRt components of HTI model. e: Ss1Rs1, Ss1Rs2, Ss2Rs1 and Ss2Rs2 components of HTI model.

2. To analyze the accuracy of calculated fracture orientations

If the subsurface is azimuthally anisotropic, unless the observation directions are parallel or orthogonal to the fracture direction, the 4C SS-wave data will each contain a mixture of S1S1- and S2S2-waves. In this case, S1S1/S2S2 separation is required for the 4C data, with results shown in Figure 1e. For the shallow layers where the fracture orientation is basically consistent, they can be regarded as an HTI medium. For the shallow layers, we can select a time window for 4C data with relatively high S/N ratio and perform shear wave splitting analysis to obtain a shallow fracture orientation. The observation directions of the 4C data are then rotated to S1-S2 directions according to the above fracture orientation. If the accurate fracture orientation is θ1 , and according to which we obtain the new 4C data, denoted as U, the accurate result of S1S1/S2S2 separation. And $\mathbf{U} = \begin{bmatrix} Ss1Rs1 & Ss1Rs2 \\ Ss2Rs1 & Ss2Rs2 \end{bmatrix} = \mathbf{R}^{\mathrm{T}}(\boldsymbol{\theta 1} - \boldsymbol{\partial})\mathbf{Q}\mathbf{R}(\boldsymbol{\theta 1} - \boldsymbol{\partial})$ (2)

For near offsets, Ss1Rs1 component (U_{11}) contains S1S1-wave，Ss2Rs2 (U_{22}) contains S2S2-waves， Ss1Rs2 and Ss2Rs1will not contain refleted waves. If the fracture orientation we obtained is inaccurate, the fracture orientation with error is denoted as θ1', that is, θ1' ≠ θ1, the obtained 4C data according to θ1' is denoted as V(θ1'), $\mathbf{V}(\boldsymbol{\theta 1'}) = \mathbf{R}^{\mathrm{T}}(\boldsymbol{\theta 1'} - \boldsymbol{\partial})\mathbf{Q}\mathbf{R}(\boldsymbol{\theta 1'} - \boldsymbol{\partial})$ (3)

Then

$$\mathbf{V}(\boldsymbol{\theta 1'}) = \mathbf{R}^{\mathrm{T}}(\boldsymbol{\theta 1'} - \boldsymbol{\theta 1})\mathbf{U}\mathbf{R}(\boldsymbol{\theta 1'} - \boldsymbol{\theta 1}) = \begin{bmatrix} \cos^2(\boldsymbol{\theta 1'} - \boldsymbol{\theta 1})\,\mathbf{U}_{11} + \sin^2(\boldsymbol{\theta 1'} - \boldsymbol{\theta 1})\,\mathbf{U}_{22} & .5\sin(2\boldsymbol{\theta 1'} - 2\boldsymbol{\theta 1})(\mathbf{U}_{11} - \mathbf{U}_{22}) \\ .5\sin(2\boldsymbol{\theta 1'} - 2\boldsymbol{\theta 1})(\mathbf{U}_{11} - \mathbf{U}_{22}) & \sin^2(\boldsymbol{\theta 1'} - \boldsymbol{\theta 1})\,\mathbf{U}_{11} + \cos^2(\boldsymbol{\theta 1'} - \boldsymbol{\theta 1})\,\mathbf{U}_{22} \end{bmatrix} \quad (4)$$

V(θ1') will has an error of S_{err}(θ1'), and

$$S_{err}(\theta 1') = \begin{bmatrix} \mathrm{Serr11} & \mathrm{Serr12} \\ \mathrm{Serr21} & \mathrm{Serr22} \end{bmatrix} = \mathrm{V} - \mathrm{U} = \begin{bmatrix} \sin^2(\theta 1' - \theta 1)\,(\mathrm{U}_{22} - \mathrm{U}_{11}) & .5\sin(2\theta 1' - 2\theta 1)(\mathrm{U}_{11} - \mathrm{U}_{22}) \\ .5\sin(2\theta 1' - 2\theta 1)(\mathrm{U}_{11} - \mathrm{U}_{22}) & \sin^2(\theta 1' - \theta 1)\,(\mathrm{U}_{11} - \mathrm{U}_{22}) \end{bmatrix} \quad (5)$$

In formula (5), let a=U_{11}-U_{22}. The value of each component of S_{err} is calculated using formula 5 and listed in table 1 when $\theta 1' - \theta 1$ equals to 1-, 2-, 5-, 10- and 20-degrees respectively.

Table 1: Value of S_{err} due to the error of θ1'

$\theta 1' - \theta 1$ (degree)	S_{err}11	S_{err}12	S_{err}21	S_{err}22
1	-0.0003a	0.0175a	0.0175a	0.0003a
2	-0.0012a	0.0349a	0.0349a	0.0012a
5	-0.0076a	0.0868a	0.0868a	0.0076a
10	-0.0302a	0.1710a	0.1710a	0.0302a
20	-0.1169a	0.3215a	0.3215a	0.1169a

The differences between Figure 2 for V(θ1') (the S1S1/S2S2 separation results with different errors of fracture orientation, from left to right, $\theta 1' - \theta 1$ equals to 1-, 2-, 5-, 10- and 20-degrees respectively) and Figure1e for U (the 4C data result with accurate value θ1) fit well with the results in Table 1. Both Table 1 and Figure 2 show that the error of fracture orientation has a greater impact on the two off-diagonal components (S_{err}12 and S_{err}21, in the orange ellipses in Figure 3) and a smaller impact on the two main diagonal components (S_{err}11 and S_{err}22, in the blue ellipses in Figure 3). Specifically: When the error of θ1' is 1 degree, there is almost no difference between the four components of V and those of U.When the error is 2 degrees, very weak reflection events appear on Ss1Rs2 and Ss2Rs1 components. When the error reaches 5 degrees, obvious reflection events appear in Ss1Rs2 and Ss2Rs1 components, while the events of Ss1Rs1 and Ss2Rs2 components are not visibly affected and remain relatively accurate. When the error exceeds 10 degrees, strong reflection events appear in the Ss1Rs2 and Ss2Rs1 components, still no obvious extra events are observed in the other two components. As the error increases to 20 degrees, obvious extra S2S2 events appear in Ss1Rs1 and extra S1S1 events in Ss2Rs2, and the quality of Ss1Rs1 and Ss2Rs2 results is no longer satisfactory, which may affect subsequent processing or interpretation.

According to the above analysis,we can judge the accuracy of the calculated fracture orientations by the presence and intensity of reflection events on Ss1Rs2 and Ss2Rs1. Additionally, the above extraneous events caused by fracture orientation errors generally do not change with azimuth especially for near offset cases, allowing judgment to be made using the 4C total stack sections added from different azimuths. Conversely, if Ss1Rs2 and Ss2Rs1 show almost no reflection energy comparable to Ss1Rs1 and Ss2Rs2, it indicates a high accuracy of the obtained $\theta 1'$.

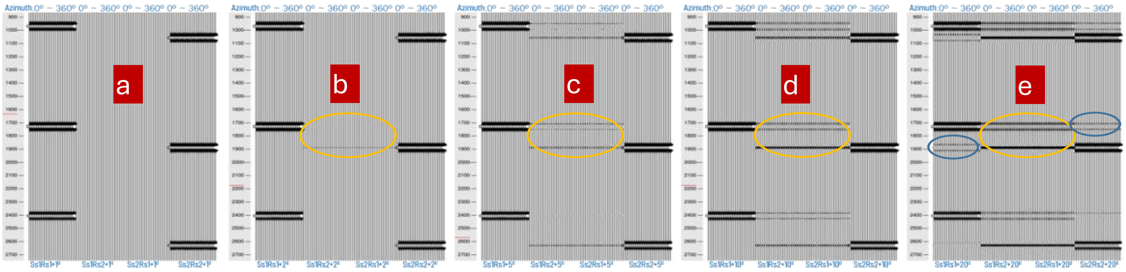

Figure 2: Common 50m offset 4C sythetic data after Alford rotation according to fracture orientation with error of 1 degree(a), 2 degrees(b), 5 degrees(c), 10 degrees(d) and 20degrees(e)

3. To determine whether fracture orientations vary with depth or not

Providing that the fracture orientation of shallow layers are accurate,that is $\theta 1' = \theta 1$ or $\theta 1' \approx \theta 1$, we still need to determine whether the fracture orientation varies with depth to decide whether to use a single-layer or multi-layer algorithm for SS-wave splitting analysis. Here, only the shallow and deep layers are considered, with the deep fracture orientation denoted as θ2. As formula (6), there is a constant (u_0) multiple relationship between U and the judgment matrix X (the definition and derivation of X and more details can be seen in the paper of Yue et al., 2021). Therefore, U can be directly used to judge whether the fracture orientation varies with depth or not.

$$\mathbf{U} = \mathbf{u_0 X} \quad (6)$$

The 4C SS-wave data from 4 models with the same θ1 but different θ2 are rotated to S1-S2 directions according to θ1 and shown in Figure 3 from left to right when θ1-θ2=0-, 30-, 90- and 120-degrees respectively. If there is also no reflected energy obviously in Ss1Rs2 and Ss2Rs1components and the time difference between S1S1 and S2S2 gradually increases with time or depth, this means the fracture orientations do not vary with depth (Figure 3a). And the discrimanation can also be made using the 4C SS-wave stack sections.

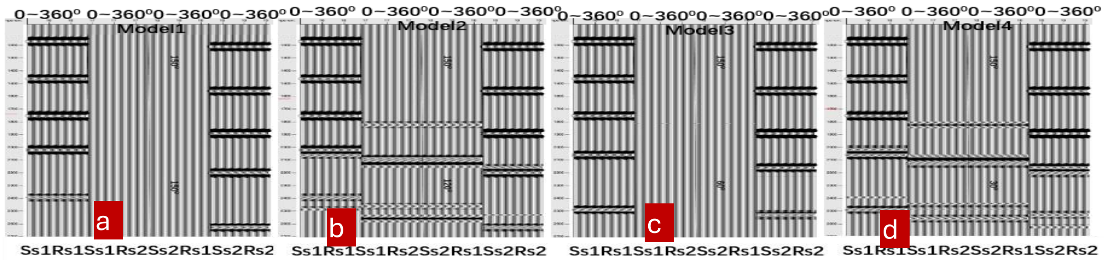

Figure 3: Common 50m offset 4C sythetic data in S1-S2 directions according to θ1 of 4 models with $\theta 1 - \theta 2$ equals to 0 degree(a), 30 degrees(b), 90 degrees(c), 120 degrees(d)

Results

After rotating the observation directions of the 4C SS-wave field data to the R-T direction, the azimuth stacked CMP gagher are shown in Figure 4a. Obvious reflections appear in SrRt and StRr components, indicating azimuthal anisotropy. After performing shear wave splitting analysis to calculate the fracture orientation for each CMP, S1S1/S2S2 separation is conducted and the results of 4C sections are shown in Figure 4c. The reflection energy of Ss1Rs2 and Ss2Rs1 is negligible compared to that of Ss1Rs1 and Ss2Rs2. This indicates that the fracture orientation θ1 is relatively accurate, and the imaging results of Ss1Rs1 and Ss2Rs2 are reliable with no extraneous events.Meanwhile, Figure 4c also shows that the fracture orientations of this sruvey varies little with depth, so S1S1/S2S2 can be separated from shallow to deep using Alford rotation.

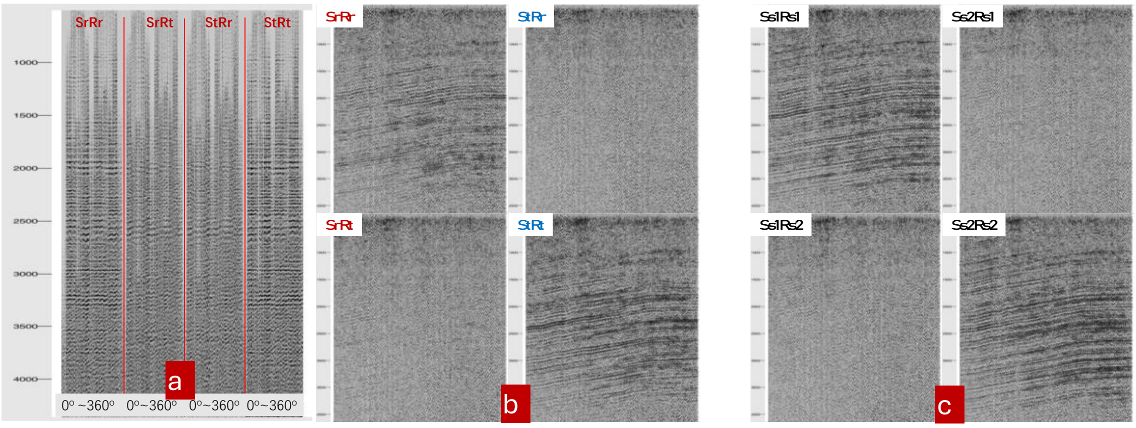

Figure 4: Results of 4C SS-wave field data. a. Azimuth stacked CMP gather in R-T directions. b. CMP stack sections in R-T directions. c. CMP stack sections in S1-S2 directions.

Conclusions

Azimuth stacked or pre-stack 4C SS-wave data in R-T directions can be used to determine whether the subsurface is azimuthlly isotropic or azimuthally anisotropic, and this is similar to the 2C PS-wave data in R-T directions. For the case of azimuthally anisotropic, the 4C data should be rotated to S1-S2 directions according to the computed fracture orientations from shallow layers for each CMP, then the obtained 4C SS-wave sections can be used to analysis the accuracy of these fracture orientations and to determine whether the fracture orientation varies with depth.

Acknowledgments

We thank BGP, CNPC for the permission to publish this paper. The research is supported by the basic research project of CNPC (2023ZZ05).

References

Alford, R., 1986, Shear data in the presence of azimuthal anisotropy: 56th Annual International Meeting, SEG, Expanded Abstracts, 476–479.

Li, X. Y., and S. Crampin, 1993, Linear-transform techniques for processing shear-wave anisotropy in four-component seismic data: Geophysics, 58,

Yue, Y. Y., P. Y. Sun, Q. G. Song, H. M. Nie, T. Q. Zhang, and J. Zhao, 2021, S1 and S2 separation based on SS wave splitting analysis: First International Meeting for Applied Geoscience & Energy, SEG/AAPG, Expanded Abstracts, 1801–1805.